International Journal of Solids and Structures 148–149 (2018) 157–168

Contents lists available at ScienceDirect

International Journal of Solids and Structures

journal homepage: www.elsevier.com/locate/ijsolstr

Imperfections and energy barriers in shell buckling

John W. Hutchinson[a,*], J. Michael T Thompson[b]

[a] School of Engineering and Applied Sciences, Harvard University, Cambridge MA 02138, UK
[b] Department of Applied Maths and Theoretical Physics, University of Cambridge, CB3 0WA, UK

ARTICLE INFO

Article history:
Revised 12 January 2018
Available online 31 January 2018

Keywords:
Buckling
Spherical shells
Cylindrical shells
Imperfections
Energy barrier
Knockdown factors

ABSTRACT

The elastic buckling of shell structures such as spherical shells subject to external pressure and cylindrical shells loaded in axial compression is highly sensitive to imperfections and often catastrophic. Recent studies of spherical shells have provided accurate quantitative results for the relation between the buckling pressure and the amplitude and shape of geometric imperfections and, additionally, quantitative results for the energy barrier that must be overcome to buckle the shell by extraneous loadings or disturbances when it is loaded to pressures below the buckling pressure. Results for the simultaneous interaction of imperfections and energy barriers for spherical shells under external pressure will be presented. Numerical studies for probing forces illustrate their use in determining the buckling energy barrier, and new experimental results on energy barriers obtained by others by probing spherical shells will be discussed and compared with predictions. It will be argued that while imperfections determine the buckling load of a shell, the energy barrier at loads below the buckling load supplies important additional information about the relative safety or precariousness of the shell to additional disturbances. Results for the energy barrier for perfect and imperfect spherical shells under external pressure provide important insights into the shell's robustness, or lack thereof, at pressures below the buckling pressure. In particular, the energy barrier trends provide critical insights into the low knockdown factor usually employed in establishing the design load of unstiffened spherical and cylindrical shells. These design loads are shown to correlate with conventional predictions provided that imperfection amplitudes scale as the shell radius.

1. Introduction

While shell buckling is not as active a research area as in was in the middle decades of the last century it seems to remain true that "everyone loves a buckling problem" (Budiansky & Hutchinson, 1979). George J. Simitses, to whom this paper is dedicated, certainly projected this attitude in his text book on buckling (Simitses & Hodges, 2006). This paper attempts to provide a unified view of two aspects of shell buckling: the enduring issue of imperfection-sensitivity and the more recently identified concept of the energy barrier to buckling. We first review recent theoretical and experimental results for the effect of dimple imperfections on the elastic buckling of spherical shells under external pressure. Then, the focus turns to the energy barrier that must be overcome by extraneous disturbances to trigger buckling of perfect and imperfect spherical shells loaded below their buckling pressure. Concomitantly, we explore some of the issues related to the employment of probing forces as an experimental technique to determine the magnitude of the energy barrier of a loaded shell (Thompson & Sieber, 2016; Hutchinson & Thompson, 2017b; Virot et al., 2017; Marthelot et al., 2017). The present paper determines the energy barrier for perfect and imperfect shells revealing that at applied pressures below about 20% of classical buckling pressure of the perfect shell the energy barrier becomes large. The conclusion to be drawn is that the shell should be able to withstand fairly large extraneous loads or disturbances when loaded at these low pressures. Conversely, when the shell is loaded to within 20% or 30% of its buckling load the energy barrier is relatively small and the shell has much less robustness to disturbances. In short, the qualitative message of this paper is that imperfections determine the buckling pressure of the shell while the energy barrier provides a measure of the shell's resistance to buckling triggered by unexpected loads or disturbances at loads below buckling.

The paper is organized with an initial focus on imperfection-sensitivity followed by a presentation of theoretical and experimental results on energy barriers and their potential 'shock-sensitivity'. Results on the imperfection-sensitivity of spherical shells subject to external pressure are presented in Sections 2 and 3. As a brief digression, Section 3 also focuses on the well-known NASA buckling knockdown factor, which is used for both spherical

* Corresponding author.
E-mail addresses: hutchinson@husm.harvard.edu, jhutchin@fas.harvard.edu (J.W. Hutchinson).

https://doi.org/10.1016/j.ijsolstr.2018.01.030
0020-7683/

shells under external pressure and cylindrical shells under axial compression. The radius to thickness dependence of this factor is examined in relation to the size-dependence of the corresponding "worse-case" imperfection amplitude. Results for energy barriers to buckling for perfect and imperfect spherical shells are presented and discussed in Section 4, with application to probing forces to trigger the buckling in Section 5. Section 5 includes some comparisons with new experimental probing measurements of the energy barrier. Section 6 compares the energy barrier for spherical shells with that obtained for cylindrical shells under axial compression by Horak et al., (2006). Section 7 presents further discussion and conclusions.

1.1. Brief historical background to the present paper

This paper derives from new insights into shell buckling that have emerged recently in the literature of nonlinear dynamical systems, substantially driven by the work of Giles Hunt and his colleagues at Bath and Bristol Universities. This research made great strides in the qualitative understanding of the localization of post-buckling patterns associated with the Maxwell load, the energy buckling load of Friedrichs (1941) (see Tsien, 1942), particularly for the axially compressed cylindrical shell. These insights were extensively reviewed by Thompson (2015), and here we would particularly single out the papers by Lord et al., (1997), Hunt et al., (2000), Hunt et al., (2003) and Horak et al., (2006).

The last of these papers (which we review in Section 6) was particularly pivotal and influential, leading fairly directly to our present work. In it, Horak and his co-workers used a novel mathematical technique to locate and quantify the lowest energy barrier against buckling for a cylindrical shell under axial compression. Drawing on this work, Thompson and van der Heijden (2014) used their background in the torsional buckling of elastic rods to demonstrate how in shell-like post-buckling a lowered energy barrier can generate a severe 'shock-sensitivity' above the Maxwell load. Meanwhile, Thompson (2015) in his review had proposed the controlled experimental probing of shells to explore, in a non-destructive way, the severity of the shock sensitivity. This was shown to be feasible by Thompson and Sieber (2016) using a simplified dynamical model of a cylindrical shell, and a historical statical model of a spherical shell. Possible problems with the technique were fully discussed, and it was shown that a bifurcation under the primary probing could be stabilized by the addition of a second rigidly controlled probe, tuned to provide zero force.

A second important source of data and stimulus came from highly accurate analyses of the post-buckling of the complete spherical shell under uniform external pressure by Hutchinson (2016). This triggered two follow-up studies of the sphere. In the first, Hutchinson and Thompson (2017a) determined energy barriers under dead, rigid and semi-rigid loading, coupled with a study of symmetry-breaking bifurcations. This work established that axisymmetric dimple buckles are stable against non-axisymmetric bifurcation until deep into the post-buckling range. These bifurcations also allowed a significant comparison with large amplitude experimental dimples with, for example, pentagonal forms. In the second study, Hutchinson and Thompson (2017b) studied the response of a pre-pressurized sphere to a point probe and its determination of energy barriers against premature collapse; again, some bifurcations from the basic axisymmetric form were observed and quantified.

We might finally note that energy barriers against the premature buckling of compressed shell structures, spheres and cylinders, have never featured strongly in the main stream of the shell-buckling literature. Some of the work that has been done is difficult to access, but we would refer the interested reader to the excellent account given by Evkin and Lykhachova (2017) and to some further discussion relevant to cylindrical shell buckling in Section 6.

2. Imperfection-sensitivity of thin elastic spherical shells under external pressure

Recent results for the effect of dimple imperfections on the buckling of elastic spherical shells drawn from Hutchinson (2016), Lee et al., (2016a), Hutchinson and Thompson (2017b) and the earlier work of Starlinger et al., (1988) will be presented briefly in this section to set the stage for the discussion of the distinct roles of imperfections and energy barriers. Attention is focused on the buckling under uniform external pressure of isotropic elastic spherical shells with radius R, thickness t, Young's modulus E and Poisson's ratio ν. Points on the middle surface of the undeformed shell are located by Euler angles with θ as the meridional angle measured from the equator and ω as the circumferential angle. Attention is initially limited to buckling behavior that is symmetric with respect to the equator, but for thin shells the localized nature of the axisymmetric dimple buckles that form at the poles is such the results are also accurate for the case of a single dimple at one pole or for hemispherical shells clamped at their equator. Initial geometric imperfections in the middle surface are assumed in the form of a slight stress-free, axisymmetric dimple focused at each pole with inward normal displacement in the form

$$w_I(\theta) = \delta e^{-(\beta/\beta_I)^2} \tag{2.1}$$

where $\beta = \pi/2 - \theta$ is measured from the pole and δ is the imperfection amplitude. The angular radius of the dimple scales according to

$$\beta_I = \frac{B}{\sqrt{\sqrt{(1-\nu^2}R/t}} \tag{2.2}$$

where for the critical imperfections B is of order unity.

The shell is subject to a net external pressure p. The classical results for the elastic buckling pressure of the perfect shell ($\delta = 0$) and the associated decrease in volume are

$$p_C = \frac{2Et^2}{\sqrt{3(1-\nu^2)}R^2} \text{ and } \Delta V_C = \frac{4\pi(1-\nu)R^2t}{\sqrt{3(1-\nu^2)}} \tag{2.3}$$

Fig. 1 displays the reduction of the buckling pressure due to the dimple imperfection, with w_{pole} as the inward normal displacement at the pole. These results have been computed with $B = 1.5$ which gives near-critical reductions of the buckling pressure over the range of imperfection amplitude plotted—see Hutchinson (2016) and Lee et al., (2016a) for computational details and further discussion of the B-dependence. Fig. 1a and b are plotted over precisely the same range, in the first plot as pressure versus pole deflection and in the second as pressure versus volume change. Due to the localized nature of the dimple buckle at the pole, the major component of the volume change as the pressure drops is the uniform expansion of the shell outside the buckled area. A detailed analysis in Section 4 of Hutchinson (2016) using a shell theory with exact bending and stretching measures reveals that at larger deflections the pressure continues to decreases monotonically until the point where the opposite poles make contact. The moderate rotation shell theory used for the calculations underlying the results in this paper is accurate for pole deflections as large as $0.2R$. Fig. 1c reveals both the extreme imperfection-sensitivity of spherical shell buckling subject to external pressure and the fact that the buckling pressure, i.e., the maximum pressure $p_{\max}$ the shell can support, plateaus to a level roughly 20% of p_C when the imperfection amplitude exceeds about one shell thickness.

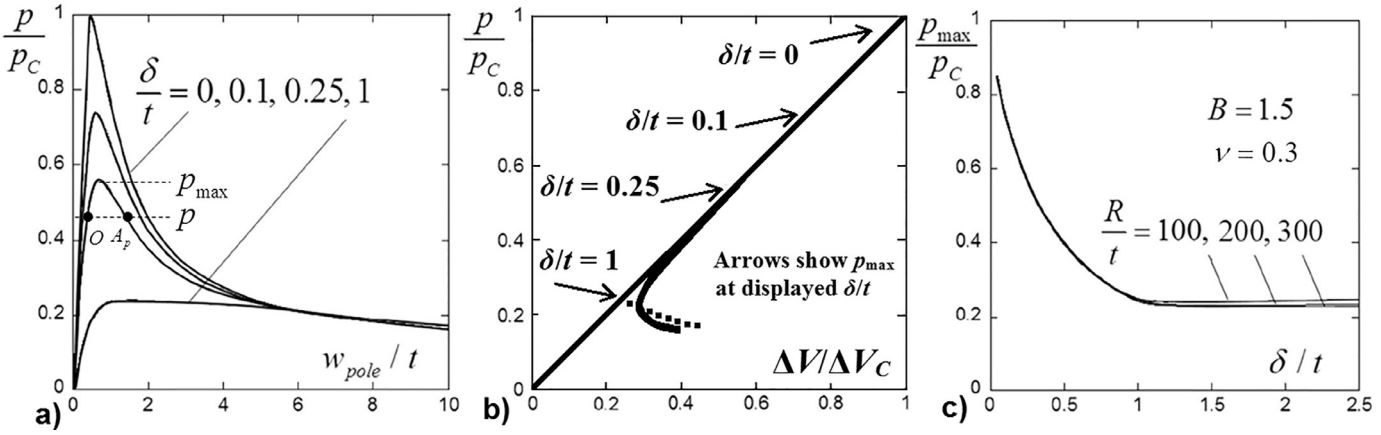

Fig. 1. (a) Pressure versus inward pole deflection for the perfect spherical shell and for three levels of imperfection. (b) Pressure versus volume chance for the same cases in (a) and plotted over the same range of buckling deflection. (c) Buckling pressure (maximum pressure) versus imperfection amplitude for three values of R/t. The results in (a) and (b) have been computed with $R/t = 200$ and $\nu = 0.3$. The results in (a), but not in (b), are essentially independent of R/t similar to those for the imperfection-sensitivity curves in (c). The results have been computed for a full sphere deforming symmetrically with respect to its equator, but results for a hemispherical shell clamped at the equator or for a full shell are almost identical.

The imperfection-sensitivity is essentially independent of R/t if $R/t > 50$ assuming the imperfection radius scales according to (2.2). The onset of the plateau of the buckling load in Fig. 1c is associated with an imperfection level that nearly flattens the shell at the pole, i.e., a curvature κ of the unloaded shell at the pole such that

$$\kappa = \left(\frac{1}{R} - \frac{1}{R^2}\frac{d^2 w_I}{d^2\theta}\right) \cong 0 \;\Rightarrow\; \frac{\delta}{t} \cong \frac{B}{2\sqrt{1-\nu^2}} \tag{2.4}$$

Most spherical shell buckling tests and applications have loading conditions that lie between the two limits of prescribed pressure (referred to by some as dead pressure) and prescribed volume change (also referred to as rigid loading). Many laboratory tests make use of water inside the shell and induce a net external pressure by reducing the volume of water within the shell. Because water can be regarded as nearly incompressible under these circumstances, such tests are inevitably much closer to prescribed volume change than prescribed pressure. The two limiting cases differ markedly in their advanced post-buckling responses—the shell snaps to a stable dimple buckle under prescribed volume change but fully collapses under prescribed pressure with the two poles making contact (within the idealizations of the modelling). These differences will be discussed further in Section 4. The dependence of the maximum pressure of an imperfect shell plotted in Fig. 1c applies to both prescribed pressure and prescribed volume change with the understanding that under prescribed volume change the pressure is a function of the prescribed volume change. Because the maximum pressure is attained at very small pole deflections (c.f., Fig. 1a), to a very good approximation, $p/p_C \cong \Delta V/\Delta V_C$ at the maximum pressure, as will be seen in Section 4. Consequently, there is only a very small difference between the pressure at instability between the two limiting loading cases. Imperfection-sensitivity results such as those in Fig. 1c are applicable whether the loading is prescribed pressure or volume change.

3. Imperfection–sensitivity trends for thin cylindrical and spherical shells

We briefly review some of the imperfection-sensitivity trends for cylindrical shells under axial compression and spherical shells under external pressure in light of the recent set of experiments carried out on spherical shells having controlled dimple imperfections (Lee et al., 2016a) and the availablity of accurate buckling predictions for these shells. One should not loose sight of the fact that these two shell/loading combinations are the most imperfection-sensitive and are thus not necessarily typical of other shells and loadings.

Fig. 2a collects in one plot three imperfection-sensitivity curves which reveal that the trends for these two shell/loading combinations are remarkably similar even though the imperfection shapes are quite different. One of the curves is Koiter's (1963) special buckling analysis for the effect of sinusoidal axisymmetric imperfections on the axial compression of cylindrical shells. Another curve, for spherical shells under external pressure, shows the effect of sinusoidal axisymmetric imperfections located near the equator of the shell, so-called belt-line imperfections (Hutchinson, 1967). The third, uppermost curve is for axisymmetric dimple imperfections in the form of (2.1) and (2.2). For the axisymmetric sinusoidal imperfections, buckling occurs as a non-axisymmetric bifurcation from the axisymmetic state. For each of these two cases, the normal displacement associated with the imperfection is given by

$$w_I = \delta \cos(\zeta x/R) \text{ with } \zeta = \left(12(1-\nu^2)\right)^{1/4}\sqrt{R/t} \tag{3.1}$$

where x is the middle surface coordinate aligned with the variation of the imperfection. Following Koiter's analysis of the cylindrical shell, the two cases, one for the cylinder and the other for the sphere, can be treated in a single analysis, and it is the outcome of this combined analysis in Hutchinson (2010) which has been used to plot the two lower curves in Fig. 2a.[1] Recent analysis in Hutchinson (2016) for complete spherical shells has confirmed the accuracy of the results in Fig. 2a for the sphere with the belt-line sinusoidal imperfections. For each imperfection amplitude, δ/t, the upper curve for the dimple imperfection in Fig. 2a is the lower envelope of the maximum pressure computed over all B in (2.2) given accurately by the fitting formula (Lee et al., 2016a):

$$\frac{p_{buck}}{p_C} = 0.68 + \frac{0.25}{0.28 + 1.05\sqrt{1-\nu^2}\delta/t} \tag{3.2}$$

For thin shells buckling elastically, each of the normalized curves in Fig. 2a is independent of R/t and ν. For the spherical shell, the belt-line sinusoidal imperfection gives a somewhat larger

[1] The formula (15) in Hutchinson (2010) for P_2 giving the bifurcation stress for both spherical shells under external pressure and cylindrical shells under axial compression is correct, but there is a misprint in the expression for b_1 given just prior to (15). The correct expression is $b_1 = \frac{1}{2}(\frac{1}{4}+\gamma^2)^{-2}[-(\frac{1}{4}+\beta\gamma^2) + \frac{c\bar{\xi}\gamma^2}{1-\sigma_1}]$ We also note that there is a misprint in Eq. (2.4) of Hutchinson & Thompson (2017a); the correct expression is $\Delta w/\Delta w_{pole} = g(\bar{s}, \xi)$.

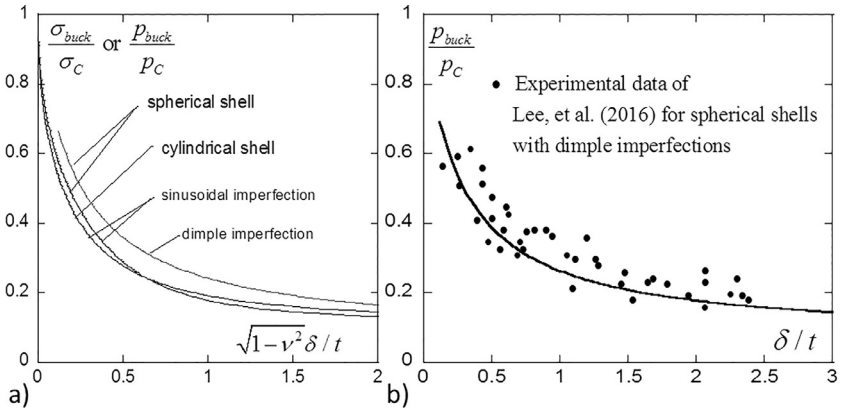

Fig. 2. Buckling stress or pressure as a function of normalized imperfection amplitude for cylindrical shells under axial compression and spherical shells under external pressure. For thin elastic shells, the numerical predictions are independent of R/t and ν. (a) Koiter's (1963) buckling stress for cylindrical shells with axisymmetric sinusoidal imperfections, buckling pressure of spherical shells with axisymmetic sinusoidal belt-line imperfections (Hutchinson 1967, 2010), and the lower envelop (3.2) of the buckling pressure for spherical shells with axisymmetric dimple imperfections (Lee et al., 2016a). (b) Experimentally measured buckling pressure for spherical shells with precisely manufactured axisymmetric dimple imperfections ($R/t = 108$, $\nu = 1/2$) subject to external pressure compared to the lower envelop of theoretical buckling pressures from a) (Lee et al., 2016a).

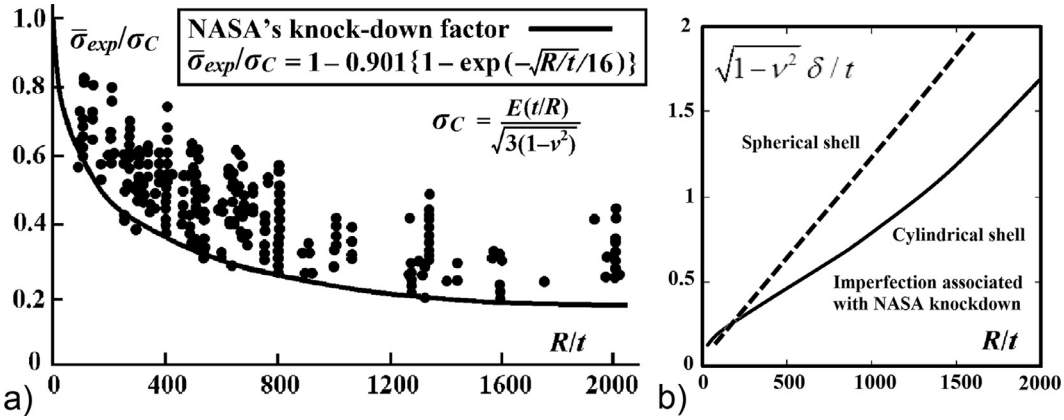

Fig. 3. Buckling of cylindrical shells under axial compression. (a) Experimental buckling data for thin cylindrical shells under axial compression collected in 1960 and plotted as the average compressive stress at buckling divided by the classical buckling stress for the perfect shell versus the radius to thickness ratio. The NASA knockdown factor used in design codes for assigning the buckling load assuming 'worse case' imperfections is shown. This factor is also frequently used for design of spherical shells under external pressure. (b) The 'worse case' imperfection amplitude corresponding to the NASA knockdown factor as a function of R/t. Koiter's result for axisymmetric imperfections in Fig. 2a is used to compute the curve for the cylinder. While (3.2) for the dimple imperfection is used to determine the curve for the sphere.

reduction in the buckling pressure than the dimple imperfection, especially in the range of small amplitudes. However, the difference between the two curves is not large and, moreover, the dimple imperfection is almost certainly the more realistic of the two imperfections shapes under most circumstances.

Fig. 2b compares the experimental results for the buckling pressure of hemispherical shells clamped at their equator having dimple imperfections in the form (2.1) at their pole from Lee et al., (2016a) with the lower envelope of the buckling predictions for the dimple imperfections. The shells are made from an elastomeric material with geometric dimple imperfections at the pole manufactured having well defined amplitude δ and polar angle β_I. The data in Fig. 2b for the tested shells have $R/t = 108$, $\nu = 1/2$ and a range of β_I. By the standards of most shell buckling comparisons, the agreement between test and theory seen in Fig. 2b is remarkably good confirming the strong link between buckling pressure and imperfection. The tests reveal the trend to plateau-like behavior for imperfection amplitudes larger than about one shell thickness.

It is well known that a dependence on R/t of the imperfection-sensitivity trends exists in the experimental data for cylindrical and spherical shell buckling. The dependence is most clearly evident in the collected experimental data presented in Fig. 3a for cylindrical shells under axial compression (Seide et al., 1960). At first glance, this dependence would appear to be at odds with the fact that the trends as plotted in Figs. 1 and 2 are independent of R/t when the imperfection amplitude is normalized by the shell thickness. However, the R/t trend of the experimental data can be explained by taking into account a dependence of the imperfection amplitude on the size of the shell. To illustate this point, consider the NASA knockdown curve plotted in Fig. 3a for the 'worse case' imperfection at any R/t,

$$\frac{\sigma_{buck}}{\sigma_C} = 1 - 0.901\left(1 - e^{-\sqrt{R/t}/16}\right), \tag{3.3}$$

and ask what imperfection amplitude gives rise to this reduced buckling stress. The result obtained using Koiter's curve in Fig. 2a for the cylindrical shell with axisymmetric imperfections is shown in Fig. 3b. The Poisson ratio associated with the many experimental points in Fig. 3a is not known, but in any case the factor $\sqrt{1-\nu^2}$ will be near unity. Because the normalised imperfection, δ/t, is almost linear in R/t in Fig. 3b, it follows that the worse case imperfection amplitude for the cylindrical shell under axial compression scales with shell radius according to $\delta \cong R/1200$.

Even though the experimental data for buckling of spherical shells under external pressure is not nearly as extensive as that for

cylindrical shells under axial compression, the NASA knockdown factor (3.3) has been commonly invoked in the design of spheres as well as cylinders. The same proceedure determining the amplidute of the imperfection for spherical shells under external pressure that gives rise to the NASA knockdown (3.3) is also presented in Fig. 3b using the lower envelop estimate (3.2) for the buckling pressure due to dimple imperfections. For the spherical shell, the "worse case" dimple-shaped imperfection amplitude has an even closer to linear dependence on the shell radius with $\delta \cong R/800$. The dimple shape of the 'worst case' imperfection for the spherical shell is almost certainly more realistic than the axisymmetric sinusoidal shapes for the other two imperfections. To our knowledge, accurate results for isolated dimple-shaped imperfections are not yet available for cylindrical shells under axial compression to use as a more representative worst case imperfection.

The fact that the worse case imperfection amplitude scales with the radius of the shell rather than its thickness makes sense, at least for some of the many processes used to manufacture shells. A wide range of imperfections can be deliberately manufactured into a shell, as demonstrated for the spherical shells of Lee et al., (2016a). The 'perfect' shells manufactured by these authors without deliberately introduced imperfections buckled in the range $0.7 < p_{buck}/p_C < 0.8$ modestly above the NASA knockdown factor for $R/t = 108$ which is about 0.6. On the other hand, the most imperfect shells of Lee et al. in Fig. 2b lie far below the knockdown factor for $R/t = 108$. Shells with relatively low radius to thickness, i.e., $R/t \approx 100$, will clearly buckle at a pressure as low as 20% of the classical pressure if their dimple imperfection amplitudes are larger than about one thickness.

One has to conclude that the various manufacturing processes for cylindrical shells representative of those collected in Fig. 3a with $R/t \approx 100$ give rise to imperfection amplitudes considerably smaller than those deliberately manufactured into the spherical shells of Lee et al., (2016a). The very thin ($R/t \cong 2000$) spherical shells manufactured and buckled under external pressure by Berke and Carlson (1968) provide another illustration of the range of perfection, or imperfection, possible for some manufacturing processes. The Berke-Carlson shells were formed by electro-plating nickel onto very accurate spherical substrates. Following the plating, some of the shells were electro-polished on the outer surface while still on the substrate yielding a highly polished, smooth surface. Several of these shells buckled at about 85% of the classical buckling pressure which is remarkable for such thin shells and far above the expectation for spherical shells with $R/t \cong 2000$. When the electro-polishing step was not employed, the shells buckled at pressures as low, or even slightly lower, than given by the knockdown factor (3.3).

4. Energy barrier to buckling for spherical shells subject to external pressure

With the background in hand from Sections 2 and 3 on the role of initial imperfections in determining the buckling pressure of spherical shells, we now ask a different question: For any shell, perfect or imperfect, loaded to a pressure below its buckling pressure, how robust is that shell to additional loads or disturbances that the shell might experience? In other words, are rather small disturbances likely to buckle the shell or will it be able to withstand substantial unespected disturbances? To gain insight into this question we examine the energy barrier to buckling at the pressure in question.

To begin, consider a loading system which prescribes the pressure p (also called pressure-control or dead loading); the other limiting case when the internal volume of the shell is prescribed (volume-control or rigid loading) will be discussed later. For any prescribed p below the maximum pressure $p_{\max}$ there are two

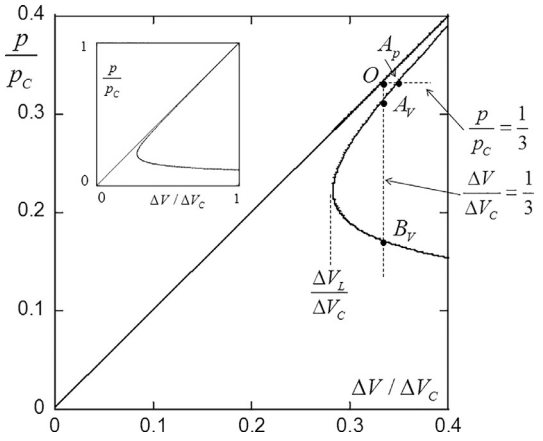

Fig. 4. Pressure versus volume change in the pre-buckling and post-buckling states for a full, perfect sphere shell that buckles symmetrically with respect to the equator and has $R/t = 200$ and $\nu = 0.3$. Loading conditions for prescribed pressure ($p/p_C = 1/3$) and prescribed volume change ($\Delta V/\Delta V_C = 1/3$) are noted. The lower limit of volume change, ΔV_L, for which post-buckling solutions exist is also noted. Under prescribed pressure the single equilibrium buckled state A_p is unstable. For prescribed volume change, with $\Delta V > \Delta V_L$ there is one unstable equilibrium buckled state A_V and one stable state B_V. The grey area sumarizes energy barrier differences as described later.

equilibrium states as illustrated in Figs. 1a and 4, the stable pre-buckling state O and the unstable buckled state A_p. State A_p is a saddle point of the energy landscape of the shell/loading system. If an extraneous loading or distrubance drives the system over this saddle point, the shell will undergo dynamic snap buckling. The energy barrier between states O and A_p, is the difference between the free energy of the shell/loading system in the two states. For prescribed p, the free energy is the strain energy in the shell plus the potential energy of the pressure loading.

The complete solution for dimple buckling of perfect spherical shells deforming symmetrically with respect to their equators given in Hutchinson and Thompson (2017a) allows us to provide explicit results for the free energy and the energy barriers of interest for the perfect shell. The solution for buckled state, $\xi > 0$, is specified by

$$\frac{p}{p_C} = f(\xi) \text{ with } \xi = \frac{\sqrt{1-\nu^2}\,\Delta w_{pole}}{t} \tag{2.5}$$

$$\frac{\Delta V}{\Delta V_C} = f(\xi) + C\frac{t}{R}h(\xi) \text{ with } C = \frac{\sqrt{3}}{(1-\nu)\sqrt{1-\nu^2}} \tag{2.6}$$

$$\frac{U}{p_C \Delta V_C} = \frac{1}{2}f(\xi)^2 + C\frac{t}{R}q(\xi) \tag{2.7}$$

Here, ΔV is the volume decrease of the shell, U is the elastic energy in the shell, and the inward buckling displacement at the pole is $\Delta w_{pole} = w_{pole} - w_0$ where w_0 is the uniform inward normal displacement in the unbuckled state at pressure p. This solution fully captures the dependence on R/t and ν and is accurate for shells with $R/t \geq 50$ as long as $\xi \leq 0.2R/t$, as further discussed in Hutchinson and Thompson (2017a) where the functions f, h and q were first tabluated. For the readers convenience, Table 1 is included below.

For the perfect shell under prescribed pressure, the difference between the free energy in state A_p and that in the unbuckled state O is readily computed using the solution (2.5)–(2.7). The dimensionless form of the energy barrier per dimple, W, for the perfect spherical shell deforming symmetrically with respect to the equator is given by

$$\frac{W}{\frac{1}{2}p_C \Delta_C C t/R} = q(\xi) - \frac{p}{p_C}h(\xi) \tag{2.8}$$

Table 1
Function values charactering dimple buckling of a perfect spherical shell determined in Hutchinson and Thompson (2017a) with ξ as the normalized pole deflection defined in (2.5). Cubic splines provide an accurate interpolation of the values listed.

ξ	$f(\xi)$	$h(\xi)$	$q(\xi)$
0	1.0000	0.0000	0.0000
1	0.6280	0.1867	0.1405
2	0.4130	0.6782	0.3840
3	0.3127	1.515	0.6795
4	0.2592	2.747	1.027
5	0.2260	4.417	1.429
6	0.2031	6.557	1.886
7	0.1858	9.186	2.395
8	0.1722	12.32	2.956
9	0.1612	15.97	3.563
10	0.1517	20.14	4.214
15	0.1209	48.92	8.058
20	0.1034	90.70	12.70
25	0.0918	145.0	17.97
30	0.0834	211.8	23.80
35	0.0770	290.8	30.12
40	0.0719	382.3	36.92
45	0.0677	486.4	44.17
50	0.0641	603.0	51.84
55	0.0611	731.9	59.91
60	0.0584	873.2	68.34

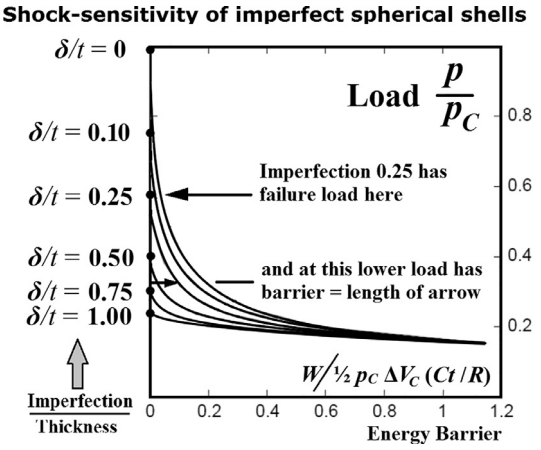

Fig. 5. The dimensionless energy barrier per dimple between the pre-buckling state O and the post-buckling state A_p for prescribed pressure p is plotted on the horizontal axis with the normalized pressure plotted on the vertical axis. Shown for the perfect shell and five levels of imperfection as measured by δ/t. The curve for the perfect shell is computed using (2.8). Those for the imperfect shells have been computed with $R/t = 200$, $\nu = 0.3$ and $B = 1.5$, but these results are essentially independent of R/t.

with ξ determined from $p/p_C = f(\xi)$. The total energy barrier for the full shell buckling symmetrically about the equator is defined as $2W$and, thus, the barrier 'per dimple' is W. The energy barrier (easily identified as an area in the pressure-volume graph) is plotted as the upper curve in Fig. 5. A different normalization of W has been used in (2.8) than that employed in Hutchinson and Thompson 2017a,b. The earlier normalization is related to that in (2.8) by

$$\frac{\sqrt{1-\nu^2}WR}{2\pi Dt} = 8\sqrt{3}\frac{W}{\frac{1}{2}p_C\Delta_C Ct/R} \tag{2.9}$$

The advantage of normalization in (2.8) is the transparent insight it provides into the magnitude of the energy barrier: $\frac{1}{2}p_C\Delta_C$ is the total elastic energy stored in the perfect shell at p_C, while the factor Ct/R scales with t/R due to the fact that the dimple buckle width scales with $\sqrt{tR}$ and thus decreases relative to the size of the shell for thinner and thinner shells. The new normalization also has the nice feature that the dimensionless energy barrier is of order unity or less in the range of interest.

Evkin and Lykhachova (2017), building on the earlier work of Evkin et al., (2016), have also presented results for the energy barrier for dimple buckling of perfect spherical shells under prescribed pressure in good agreement with the upper curve in Fig. 5. The dimensionless energy barrier in their paper is denoted by $\bar{\Pi}$ and is equal to dimensionless barrier in (2.8) times the factor $4/\sqrt{3(1-\nu^2)}$. The work presented in Evkin and Lykhachova (2017) includes both finite element computations and asymptotic analytical formulas for the energy barrier. As is being argued in this paper, these authors asert that the trend for the energy barrier with p/p_C provides a rationale for the design pressure of roughly 20% of p_C employed in many codes for thin spherical shells under external pressure. These authors also present an illustration of the insensitivity of dimple buckling to its location on the shell by showing that a dimple in state A_p that forms between the pole and equator is identical to an axisymmetric dimple formed at the pole. Of course, identical behavior must be expected given the highly localized nature of dimple buckling, but it is reassuring to see this emerge directly from one numerical analysis that is axisymmetric and the other that is not.

Computation of the energy barrier with p prescribed for five levels of imperfection are also shown in Fig. 5 providing comparison with the energy barrier for the perfect shell. These results, as well as the previously unpublished results in Section 5, have been computed using the numerical method detailed in Hutchinson and Thompson (2017b) and Hutchinson (2016). Two features of the barrier plots in Fig. 5 stand out. (1) For perfect or near perfect shells the energy barrier at pressures in a substantial range below the maximum below $p_{\max}$ remains very low. (2) For lower pressures around $p/p_C = 0.2$ the energy barrier becomes large and, moreover, is only weakly dependent on the imperfection amplitude. It seems reasonable to assert that shells with small imperfections will not be robust against buckling if loaded anywhere near the buckling pressure while, conversely, shells loaded at pressures at about 20% of p_C will be quite robust and nearly independent of $p_{\max}$ as long as $p_{\max}$ is not itself as low as 20% of p_C.

As already noted, there are significants differences between the post-buckling behavior in the two limiting loading cases, prescribed pressure and prescribed volume change. Under prescribed pressure the buckled shell snaps dynamically to a collasped state with the two poles making contact (Hutchinson, 2016). By contrast, under prescribed volume change the shell snaps to a stable dimpled state (Hutchinson & Thompson, 2017a,b). In the latter case, the net pressure acting on the shell decreases abruptly as the shell buckles thereby giving rise to a stable dimple buckle. This difference is brought out in Fig. 4 where the pre-buckling and post-buckling behavior is plotted in the form of pressure versus change in volume for the perfect spherical shell. For the unbuckled shell, $p/p_C = \Delta V/\Delta V_C$ in state O for both loading cases. As already discussed, under prescribed pressure there is only one equilibrium buckled state, A_p, and it is unstable. Under prescribed volume change with $\Delta V > \Delta V_L$, there are two equilibrium states, A_V, which is unstable, and, B_V, which is stable. When the shell buckles under prescribed volume change it snaps to state B_V.

Under prescribed volume change the free energy of the system is simply the elastic energy in the shell, and the energy barrier to buckling is the difference between the free energy in states A_V and O. For the perfect shell, the energy barrier per dimple, W, can again be computed using (2.5)–(2.7) with the result

$$\frac{W}{\frac{1}{2}p_C\Delta_C Ct/R} = q(\xi) - \frac{\Delta V}{\Delta V_C}h(\xi) + \frac{1}{2}C\frac{t}{R}h(\xi)^2 \tag{2.10}$$

where $\xi \equiv \xi_A$ is given in terms of $\Delta V/\Delta V_C$ by (2.6) as now described. For any Ct/R there is a lower limit of $\Delta V/\Delta V_C$, denoted

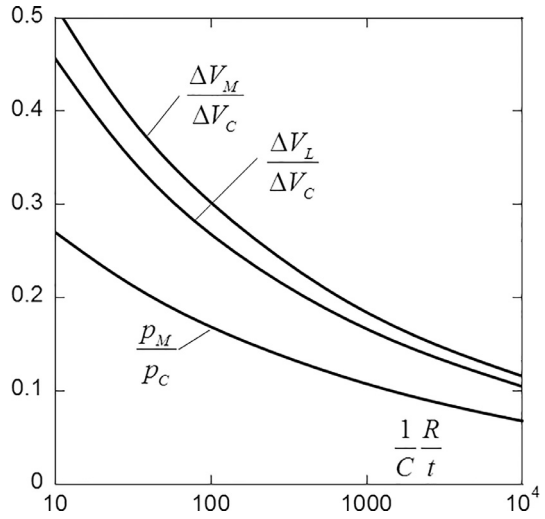

Fig. 6. The R/t-dependence of three quantities for perfect spherical shells subject to prescribed volume change: The upper curve is the prescribed volume change associated with the Maxwell equal energy criterion and the lower curve is the associated pressure in the stable post-bucking equilibrium state. The middle curve is the lower limit of prescribed volume change for which post-buckling equilibrium states exist. These curves apply for shells deforming symmetrically about the equator with equal dimple buckles at the top and bottom poles.

by $\Delta V_L/\Delta V_C$ and plotted in Fig. 6, for which positive values of ξ satisfying (2.6) exist. For prescribed $\Delta V > \Delta V_L$, two values of ξ satisfying (2.6) exist, one associated with state A_V, denoted by ξ_A, and the other associated with B_V, denoted byξ_B. The energy barrier for prescribed $\Delta V/\Delta V_C$ computed from (2.10) with $\xi \equiv \xi_A$ is plotted for several values of $C\,t/R$ in Fig. 7a, in each case over the relevant range $\Delta V_L < \Delta V < \Delta V_C$. The limit for very thin shells, $C\,t/R \to 0$, coincides with the result for prescribed pressure with $p/p_C \to \Delta V/\Delta V_C$, as can be seen directly from (2.8), (2.10) and (2.6).

The difference between the energy in the stable dimple state B_V and that in state O is denoted by W_B and is determined by (2.10) with $\xi = \xi_B$. Again, this energy difference is easily identified as an area in the pressure-volume graph; it is plotted in Fig. 7b. Another aspect of prescribed volume change brought out in Fig. 7b is the existence of stable equilibrium buckled states B_V with energy equal to that in the unbuckled state O, i.e., $W_B = 0$. These are the Maxwell equal energy states. The prescribed volume change, ΔV_M, and associated pressure in the buckled state, p_M, for the Maxwell states are plotted as a function of $R/C\,t$ in Fig. 6. For $\Delta V < \Delta V_M$ the energy in the unbuckled state is less than that in state B_V, while for $\Delta V > \Delta V_M$, the energy in the unbuckled state is greater than that in B_V. Elastic systems with these characteristics display hysteritic behavior when loading histories are imposed causing the shell to undergo cycles snapping back and forth between buckled and unbuckled states. Such equal energy states do not exist under prescribed pressure, assuming one excludes the collapsed states of the shell.

An important conclusion to be drawn from these results is that there is relatively little difference between the buckling energy barrier under prescribed volume change from that under prescribed pressure, other than the existence of the lower limit of prescribed volume change for which buckling can occur. Indeed, the difference simply coresponds to the small grey-shaded area in Fig. 4. The small difference is also clearly evident when one compares the barrier curves in Fig. 7a with that in Fig. 5 for the perfect shell. Anologous to the conclusion noted earlier regarding buckling imperfection-sensitivity, the energy barrier for spherical shells under external pressure is only weakly dependent on the compliance of the system applying the pressure. These conclusions stem from the fact that both the imperfection-sensitivity and the energy barrier are established in the range of relatively small buckling deflections. By contrast, the advanced post-buckling behavior is vastly different for the two cases with prescribed pressure producing collapse and prescribed volume change giving rise to a stable, finite-sized dimple. Finally it is worth noting that, due to the localized nature of the dimple buckle and its relatively small size, the results presented in the figures in this section can also be applied to a clamped hemispherical shell with a single dimple at the pole or to a full spherical shell with only one dimple buckle. For thin shells, clamping at the equator has almost no influence on the dimple buckle as long as it is well away from the equator, as has been established here by numerical calculation of the two cases. Thus,

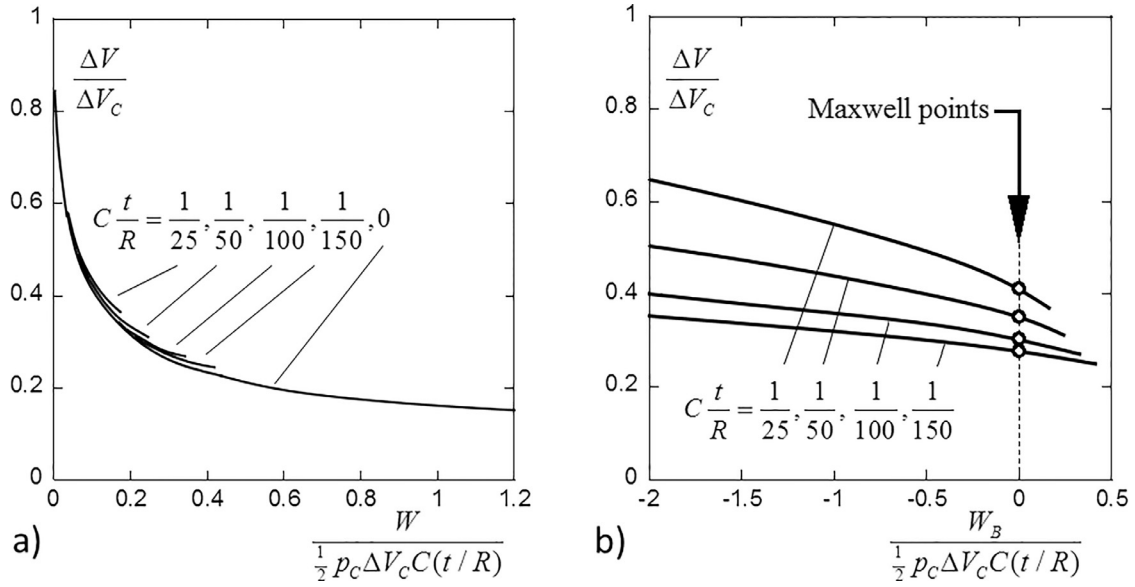

Fig. 7. (a) Dimensionless energy barrier per dimple for the perfect shell for prescribed change of volume $\Delta V/\Delta V_C$ for various values of $C\,t/R$. The lower limit $\Delta V_L/\Delta V_C$ (plotted in Fig. 6) depends on $C\,R/t$. (b) The difference in the energy per dimple for prescribed volume change between the stable post-buckling state B_V and the pre-buckling state O. The value of $\Delta V/\Delta V_C$ associated with the Maxwell state M at which the energy in states O and B_V are equal is marked (see also Fig. 6). These curves apply for shells deforming symmetrically about the equator with equal dimple buckles at the top and bottom poles.

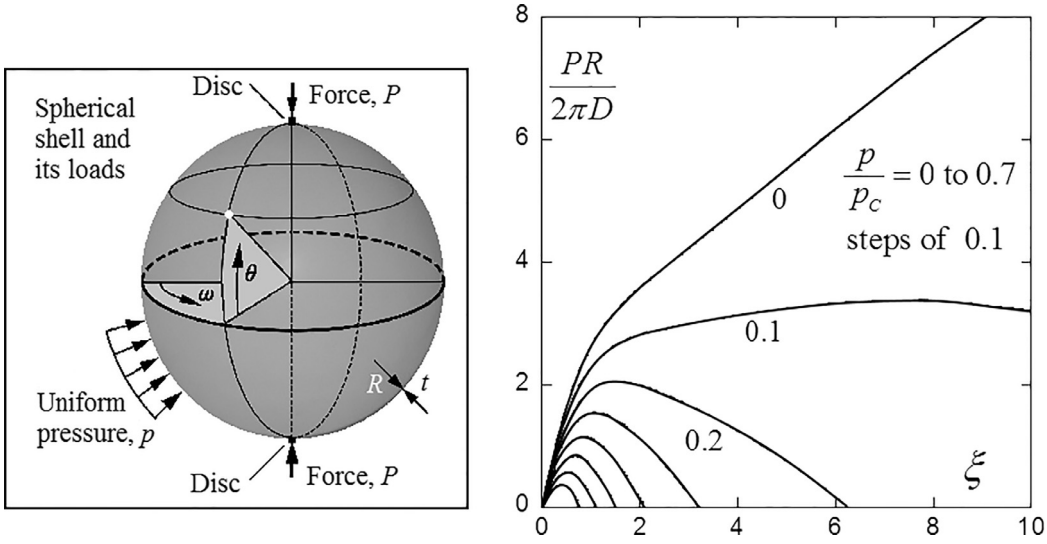

Fig. 8. Perfect spherical shell loaded under prescribed pressure p and then subject to equal and oppositely-directed pole probe forces P. For pressures in the right hand plot having $p/p_C > 0.14$, the probe force becomes zero at the intersection with the pole deflection axis ξ. The deformations in this plot are axisymmetric. The zero crossing is the unstable post-buckled equilibrium state A_p. The work done by the probing force to reach A_p (the area under the curve) is equal to the energy barrier W. The shell has $R/t = 200$ and $\nu = 0.3$ but the curves are essentially independent of R/t. (from Hutchinson & Thompson (2017b).

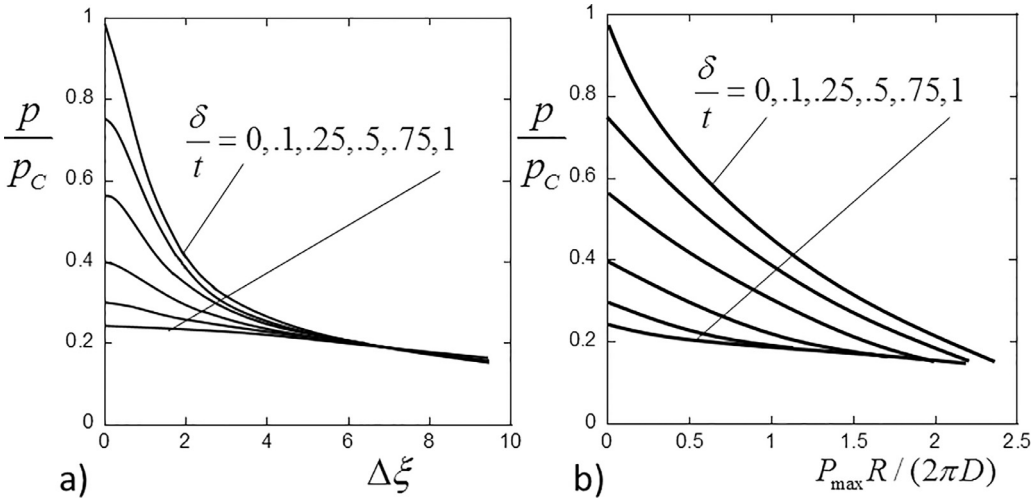

Fig. 9. For various levels of imperfection, the dimensionless additional pole deflection $\Delta\xi$ produced by the probing force at attainment of the unstable state A_p in (a) and the maximum probing force $P_{\max}$ in (b). The associated energy barrier curves are presented in Fig. 5. These results have been computed for shells with $R/t = 200$. $\nu = 0.3$ and $B = 1.5$ but they are essentially independent of R/t.

all the results can be applied directly to the hemisphere with ΔV and ΔV_C being half the values for the full shell. For full spherical shells with one dimple buckle, the solution (2.5)–(2.6) continues to hold if C is replaced by $C/2$, with a similar substitution in Fig. 6.

5. Probing the shell's energy barrier and its shock-sensitivity

5.1. Numerical predictions

An example which illustrates the role of the energy barrier is the effect of applying inward radially-directed probing forces P to the poles of a spherical shell loaded to pressure p as analyzed by Hutchinson and Thompson (2017b) and shown for a perfect spherical shell in Fig. 8. In this figure, for shells pre-loaded to $p/p_C > 0.14$ with p subsequently held fixed (prescribed pressure), the probe force increases to a maximum, $P_{\max}$, and then declines to zero. The solution at $P = 0$ with $\xi > 0$ is the unstable post-buckling equilibrium point of the perfect shell at state A_p given by $p/p_C = f(\xi)$; this unstable state can be stabilized by a suitably controlled probe as discussed thoroughly by Thompson and Sieber (2016). Moreover, the work done by the probe force through the pole deflection is precisely the energy barrier W given by (2.8). The probing behavior for prescribed pressure satisfying $p/p_C > 0.14$ is axisymmetric over the entire range shown in Fig. 8. If $p/p_C < 0.14$, the probing behavior is more complicated with non-axisymmetric bifurcation occurring prior to attainment of $P = 0$ (Hutchinson & Thompson, 2017b).

Fig. 9 presents results for shells with identical dimple imperfections at each pole, loaded under prescribed pressure, and then subject to equal and opposite probing forces at the poles at the centers of the dimple imperfections. The additional dimensionless pole deflection, $\Delta\xi = \xi_{A_p} - \xi_O$, due to the probe force at the point where $P = 0$ at state A_p is plotted in Fig. 9a, and the maximum value attained by the probe force is presented in Fig. 9b. As in the case of the perfect shell, the state at $P = 0$ is the same unstable post-buckled equilibrium state A_p identified for the shell subject to pressure alone. Thus, it follows that the work done by the probing force must necessarily equal the energy barrier W presented in Fig. 5, as has indeed been verified. Like the energy barrier it-

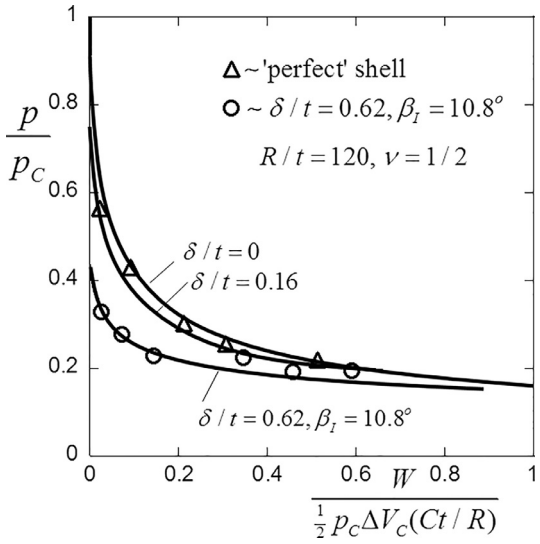

Fig. 10. Experimental measurement of the energy barrier by probing hemispherical shells clamped at the equator that are subject to prescribed pressure p (Marthelot et al., 2017). One shell is nearly perfect and the second shell has a manufactured dimple imperfection at the pole with amplitude $\delta/t = 0.62$ and $B = 1.92$. Further details are discussed in the text. The theoretical curves are computed with $R/t = 120$ and $\nu = 1/2$.

self, the additional pole deflection of the probe required to trigger buckling is small (less than a shell thickness) for shells with small imperfections loaded to pressures within about 25% of the buckling pressure. However, the pole deflection becomes relatively large and nearly independent of the imperfection when p/p_C is around 0.2.

5.2. Experimental results from probing the energy barrier

Systematic experimental results on probing loaded shell structures to trigger buckling have only recently been carried out. A study probing axially loaded cylindrical shells has been carried out by Virot et al., (2017) with a few of their preliminary results previously reported by Hutchinson and Thompson (2017b). An extensive experimental study of the technique of probing spherical shells subject to external pressure has been performed by Marthelot et al., (2017). Here we present the measured energy barrier for two of the spherical shells probe tested by these authors.

The shells are elastomeric hemispheres clamped at their equators. The process of manufacturing the shells is described in Lee et al., 2016b with details of how a precise dimple imperfection at the pole can be introduced described in Lee et al., (2016a). The 'perfect' shells, manufactured with no deliberately introduced imperfection, buckle in the range of $0.7p_C$ to $0.8p_C$. A systematic buckling imperfection-sensitivity study under pressure alone was presented in Lee et al., (2016a). The two shells for which experimental data is presented in Fig. 10 have $R/t = 120$ and $\nu = 1/2$. One shell is 'perfect' in the sense described above which buckled under pressure alone at $0.74p_C$ with a dimple buckle occurring well away from the pole. The other shell was manufactured to be imperfect with a dimple shape at the pole approximated by (2.1) with $\delta/t = 0.62$ and $\beta_I = 10.8^o$ ($B = 1.92$). The experimental loading system was designed to apply prescribed pressure while the probe was applied under conditions of prescribed displacement. The experimentally measured energy barrier (e.g., the work done by the probe to reach the unstable equilibrium state A_p) at various levels of prescribed pressure is presented in Fig. 10 for each of the two shells. Good agreement with numerical predictions computed for these shells is evident. The predictions in Fig. 10 have been computed for both clamped hemispheres and full spherical shells subject to symmetry conditions at the equator with no discernable difference between the two sets of results. An imperfection amplitude $\delta/t = 0.16$ produces a buckling load under pressure alone of $0.74p_C$ corresponding to that of the 'perfect' shell and a theoretical curve for this imperfection is also shown.

The insensitivity to conditions at the equator emphasizes the highly localized nature of dimple buckling for the spherical shell. Further evidence of the localized nature of buckling is the fact that under pressure alone the 'perfect' shell undergoes dimple buckling well away from the pole, no doubt associated with some small unidentified imperfection at that location. Nevertheless, Marthelot et al., (2017) report that for each of the five data points in Fig. 10 for the 'perfect' shell the probe triggers a dimple buckle at the pole not at that other location. The unidentified imperfection is probably too far from the pole to interact with the probe.

5.3. Probing at locations remote from a dimple imperfection

For spherical shells under external pressure the energy barrier for a shell with a dominant imperfection is only relevant if the probe or other disturbance is applied sufficiently near the imperfection so as to trigger buckling at the imperfection. By analyzing a simple example in this section, we will illustrate that a full shell with a single dimple imperfection will behave as if it were a perfect shell at applied pressures below the buckling pressure when probed well away from the imperfection. Because our present numerical method is limited to axisymmetric deformations we consider a full spherical shell with a single dimple imperfection at the upper pole and otherwise perfect. This shell is then probed with equal and opposite forces at the poles, and the work exerted by the probe system to buckle the shell is computed. One case (shell B) has equal and opposite concentrated forces at the poles, while the other case (shell C) has a concentrated probing force at the lower pole and a broadly distributed normal pressure with an equal and opposite resultant force at the upper pole. The pressure at the upper pole for shell C is distributed in proportion to $e^{-(\beta/\beta_p)^2}$ with $\beta_p = 3\beta_I$ such that the additional pressure resisting the probe at the upper pole is very small compared to the applied uniform pressure p. Results for the energy barrier perfect shell (shell A) are also included for comparison.

The shells in Fig. 11 have $R/t = 100$ and $\nu = 0.3$. The upper pole imperfection of shells B and C have $\delta/t = 0.5$ and $B = 1.5$. Under uniform pressure alone, shells B and C undergo dimple buckling at the upper pole at a buckling pressure $p/p = 0.39$. The curve for the dimensionless energy barrier for shell B in Fig. 11 is essentially identical to that presented for the energy barrier per dimple in Fig. 5 for a shell with similar dimple imperfections at each pole and undergoing symmetric buckling about the equator. The dimensionless energy barrier of the perfect shell A in Fig. 11 is also essentially identical to that for the perfect shell in Fig. 5 for the energy per dimple. For shell A, $W$is taken to be the barrier at the upper pole. As noted earlier, if the perfect shell buckles symmetrically respect to the equator with a buckle at each pole, as in the computations for Fig. 5, the total energy barrier is $2W$. However, if a very small imperfection triggers buckling first at the upper pole then that buckle localizes and grows while a buckle at the lower pole will not form; the energy barrier of the full perfect shell is then W not $2W$. This is the relevant barrier for the present comparison. At prescribed pressures below the buckling pressure, i.e., $p/p < 0.39$, probing of shell C causes buckling at the lower pole even though the imperfection is at the upper pole. As seen in Fig. 11, the work exerted by the probing system for shell C is essentially identical to the energy barrier per dimple for the perfect shell. This behavior is not unexpected because of the localized nature of the buckling and because the probing system only increases the pressure at the

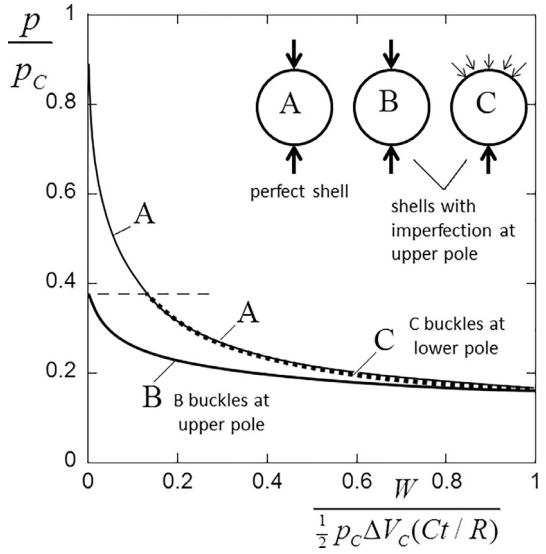

Fig. 11. Energy barrier determined by probing three full spherical shells with $R/t = 100$ and $\nu = 0.3$. Shell A is a perfect shell probed by equal and opposite forces at the poles. For this case W is the barrier per pole—see further discussion the test. Shells B and C have identical dimple imperfections ($\delta/t = 0.5$ and $B = 1.5$) at the upper pole with no imperfection at the lower pole. The buckling pressure for shells B and C subject to pressure alone is indicated by the horizontal line at $p/p_C = 0.39$. Shell B is probed by equal and opposite forces at the poles, and it buckles at the upper pole with the energy barrier shown. Shell C is probed by a concentrated force at the lower pole and is opposed by a broadly distributed pressure centered at the top pole which has equal and opposite force resisting the probe force at the lower pole (see text for details). At pressures below $p/p_C = 0.39$, shell C buckles at the lower pole with an energy barrier identical to that of the perfect shell.

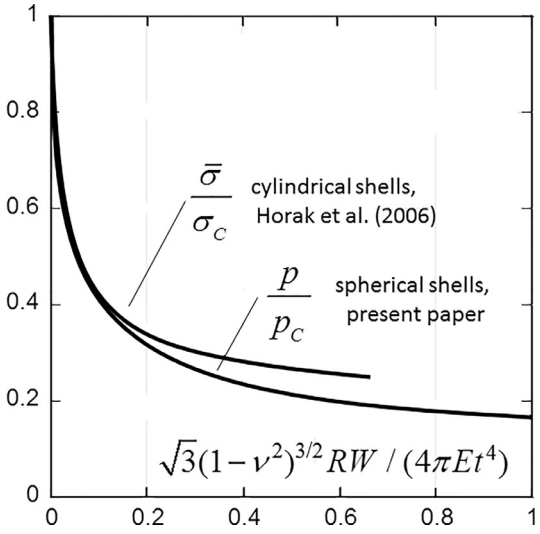

Fig. 12. Comparison between the energy barrier W to buckling of cylindrical shells under axial compression (Horak et al., 2006) and spherical shells under external pressure. The normalization of energy barrier plotted on the horizontal axis is the same as that in (2.8) and in Figs. 5 and 7 with R as the radius of the sphere or cylinder, respectively, and t as the shell thickness. The curve for cylindrical shells was plotted by using (6.1) and reading values of $V(\lambda)$ from Fig. (4.3) in Horak et al., (2006).

upper pole very slightly. Once the applied pressure p attains the buckling pressure, $p/p = 0.39$, the energy barrier vanishes and shell C undergoes snap buckling at the upper pole.

An abrupt transition occurs between buckling at the lower pole triggered by the probe and buckling at the upper pole produced by the uniform applied pressure. We have not attempted to resolve this transition more finely that the plot in Fig. 11 reveals, where the largest pressure for which buckling at the lower pole was computed is $p/p_C = 0.37$. While the example in this section is relatively simple, it highlights two lessons concerning probing and energy barriers which are likely to be broadly relevant for shells. The first lesson is the more positive of the two. When the probe or disturbance is not directed sufficiently near the worst imperfection, the energy barrier for buckling is greater than the barrier associated with buckling at the imperfection. The second lesson is that if one's aim is to use a probing technique to experimentally measure the energy barrier by extrapolating to the buckling limit using data at loads below the buckling limit, then one has to be sure to probe sufficiently near the most dilatory imperfection if one expects to measure the lowest energy barrier. Each of these lessons stems from the localized nature of shell buckling for this type of shell/loading system.

6. Energy barrier for cylindrical shells under axial compression

Significant efforts are currently underway in Europe, the United States and in China to revise the design criteria for cylindrical shells under axial compression to break away from use of the NASA knockdown factor (3.3), which is regarded by many as being too conservative for well-constructed shells. The new approaches still make use of experimental verification but also employ a more heavy reliance on computational buckling work, incorporating realistic imperfections (Haynie et al., 2012; Krasovsky et al., 2011; Wagner et al., 2017; Wang et al., 2013). Several avenues are being pursued, including the use of lateral probing forces or displacements as surrogate imperfections and attempts to identify and compute a meaningful lower bound to the buckling load. Some of these ideas derive from early buckling research carried out in the former Soviet Union (e.g., Mossakovskiy et al., 1975; Evkin et al., 1978). A number of aspects underlying these new approaches are still in a state of flux and new design criteria for shell buckling are not yet in place. Suffice it to say that the outstanding research issues needed to advance the new criteria center, at least in part, on imperfection-sensitivity and the role of probing.

The cylindrical shell energy barrier problem is more challenging than the spherical shell problem because the former is inherently two-dimensional while the latter is axisymmetric for dimple buckling and thus one-dimensional. A ground-breaking analysis of the energy barrier for perfect, elastic cylindrical shells under axial compression has been carried out by Horak et al., (2006). For perfect cylindrical shells of radius R and thickness t loaded to an average compressive axial stress $\bar{\sigma}$ less than the classical buckling stress, i.e., $\bar{\sigma}/\sigma_C < 1$ with $\sigma_C = Et/(\sqrt{3(1-\nu^2)}R)$, these authors computed the energy difference W between the energy in the unbuckled state and that at the lowest saddle point, or 'mountain pass' as the authors call it. This lowest mountain pass was shown by a mathematical search routine to be associated with a dimple-like buckle (localized both axially and circumferentially) having a characteristic width and height of order $\sqrt{Rt}$. The central result of Horak et al., (2006) can be expressed as

$$\frac{\sqrt{3}\left(1-\nu^2\right)^{3/2}RW}{4\pi Et^4} = \frac{1}{96\pi}V(\lambda) \tag{6.1}$$

where, in their notation, $\lambda = 2\bar{\sigma}/\sigma_C$ and $V(\lambda)$ is plotted in their Fig. 4.3. The normalization of W in (6.1) is identical to that introduced in (2.8) and used in Figs. 5 and 7 but expressed here directly in terms of the shell and material parameters which hold for both shells. As in the case of the results in the present study of spherical shells there is no additional dependence on R/t or ν for thin shells. The energy barrier (6.1) for the cylindrical shell subject to prescribed average axial compression is compared to the barrier for the spherical shell subject to prescribed pressure in Fig. 12.

The similarity of the energy barrier for the two shell/loading systems seen in Fig. 12 is gratifying but not entirely unexpected given the long standing experience based on experimental data for these two systems that their buckling behavior is similarly imperfection-sensitive and catastrophic. Moreover, the NASA knockdown factor (3.2) which was developed based on experimental data for cylindrical shells is often applied to spherical shells, notwithstanding that the experimental data set for spherical shells is not as large. A further complication for cylindrical shells versus spherical shells is the various choices of boundary conditions which can be assumed for the cylindrical shell. Horak et al., (2006) invoke boundary conditions in their analysis which might be described as being among the least stiff of conditions representative of tests used to generate experimental data or for structural applications. For example, for the limit of prescribed displacement, referred to as the constrained case by the authors, a uniform axial displacement at the ends of the cylinder is not imposed, as would be the most realistic assumption for modeling most test situations. Instead, the authors impose the average axial displacement of the ends allowing the axial displacement to become non-uniform at the ends in the buckled shell. This end condition flexibility might contribute to some relaxation of the in-plane compression experienced by the dimple buckle and might even allow the shell ends to tilt relative to one another. For the other limit, the average axial stress (the axial load) is prescribed which is work conjugate to the average axial displacement. For both these limiting cases, the authors assume the shell is free to slide circumferentially at the ends. Some influence of these boundary conditions on the energy barrier plotted in Fig. 12 is expected, including the possibility that the imposition of the average axial displacement rather than uniform axial displacement may explain the fact that the energy barrier for the cylindrical shell is somewhat larger than that of the spherical shell.

Another interesting observation related to the work of Horak et al., (2006) is their tentative conclusion, based on their numerical results, that there appears to be no difference between the energy barriers under prescribed axial load and prescribed average end shortening. Recall that the present results for the perfect spherical shell under the two limiting conditions of prescribed pressure and prescribed volume change (c.f., Eqs. (2.8) and (2.10) and Figs. 5 and 7) have a small difference which vanishes as $R/t \to \infty$. We expect similar behavior for the cylindrical shell: a small difference due to the fact that under prescribed end-shortening the average axial load diminishes as buckling occurs. The analog to spherical shell buckling carries over to the advanced post-buckling behavior. Under prescribed axial load, buckling should lead to complete collapse of the cylinder, while under prescribed end shortening the shell is expected to snap to a stable state with one or more dimples. It is also reasonable to expect that the effect of geometric imperfections on the energy barrier for the cylindrical shell will be similar to that found here for spherical shells.

In summary, as the remarks above on the buckling energy barrier for the cylindrical shell under axial compression suggest, there are open questions related to the boundary conditions that need further resolution. The experimental boundary conditions of most recent laboratory tests are probably represented most closely as being clamped ends with prescribed uniform end-displacement, and it is important that this limiting set of boundary conditions is properly modeled in the energy barrier and probing simulations. A recent analysis of the dimple buckle state at the mountain pass by Kreilos and Schneider (2017) also invokes a set of boundary conditions that is difficult to relate to conditions relevant to either laboratory tests or to applications. For both the determination of energy barriers and probing responses, it is equally important that attention be addressed to boundary conditions that are relevant to applications such as launch vehicles for which fully clamped ends with prescribed uniform end-shortening is almost certainly an unrealistically stiff set of conditions. It is possible that the stable isolated dimples induced by probing that are observed in some of the experiments employing the maximally stiff boundary conditions may be unstable, or even non-existent, for other boundary conditions, as illustrated in the case for the spherical shell for the two limits of prescribed pressure and prescribed volume change.

7. Concluding remarks

Based on the numerical results for dimple buckling and associated energy barriers of spherical shells subject to external pressure, we have argued that for this system imperfections determine the reduction of the buckling pressure below the classical buckling pressure while the energy barrier determines the robustness, or lack thereof, of the shell to unanticipated disturbances at pressure loads below the buckling pressure. For perfect shells, or shells with relatively small imperfections, the energy barrier is very small in a substantial pressure range below the buckling pressure. The barrier increases to much larger values for p/p_C around 0.2. The energy barrier trends in Fig. 5 have several implications. For example, even if one could manufacture near-perfect spherical shells, one would be reluctant to load them at pressures close to the buckling pressure unless one were absolutely certain that the shell would not experience unexpected disturbances. Conversely, even for spherical shells with modestly large imperfections, e.g., $\delta/t \cong 0.5$ in Fig. 5, one could still be confident that a shell loaded to $p/p_C \cong 0.2$ would have substantial resistance to disturbances. Taken together these two implications add to the rationale for the buckling knock-down factor of $\approx$ 0.2 widely adopted in the design of thin spherical shells under external pressure. Evkin and Lykhachova (2017) make a similar argument based on their energy barrier results for perfect spherical shells.

An important finding is that the energy barrier to buckling of the spherical shell under external pressure has only a weak dependence on the compliance of the loading system applying the pressure. The difference between the energy barriers in the limiting cases of prescribed pressure and prescribed volume change is quite small. In this regard, the energy barrier is similar to the buckling pressure itself. The earlier calculations of Horak et al., (2006) for cylindrical shells under axial compression, although somewhat more tentative on the issue, come to the same conclusion.

Probing a loaded shell at the right location can be implemented as an experimental technique to measure the energy barrier (Virot et al., 2017; Marthelot et al., 2017). Moreover, in principle, it may be possible to develop an experimental protocol to nondestructively measure the buckling load of the shell by carefully probing at a sequence of load levels and then extrapolating to the point of buckling. The example discussed in Section 5 cautions that developing such a protocol is not likely to be straightforward and it will almost certainly depend critically on probing a shell near its most vulnerable location.

To our knowledge, there are no results available for buckling energy barriers for shell problems other than those discussed in this paper. Stiffening generally reduces the imperfection-sensitivity of shells in the sense that for common methods of manufacture the reduction of the buckling load relative to that of the perfect shell is often less than that for unstiffened shells. It would be interesting to know if there is a corresponding increase in the energy barrier for stiffened shells at loads not far below the buckling load. Insight to this question can be obtained in a simple, straightforward manner for the bending stiffness enhancement associated with isotropic sandwich shells. For either the spherical or cylindrical shell we will compare a monocoque shell with ra-

dius R, thickness t, Young's modulus E and Poisson's ratio ν with an isotropic sandwich shell of the same radius, same areal mass and whose material has the same Young's modulus and Poisson's ratio. To keep things as simple as possible, we will assume that the fraction of the material in the core of the sandwich can be neglected such that each face sheet has thickness $t/2$. With c as the distance between the inner surfaces of the two face sheets, it is straightforward to show (assuming Kirchhoff-Euler-Bernoulli kinematics apply) that the sandwich has the same bending and stretching stiffness as a monocoque shell with an effective modulus $E_{eff} = E/\sqrt{1+3(c/t)+3(c/t)^2}$ and an effective thickness $t_{eff} = t\sqrt{1+3(c/t)+3(c/t)^2}$. (Note that the limit with $c \to 0$ are those of the monocoque shell.) It follows, that all the results derived for the monocoque shell in this paper apply to the isotropic sandwich shell if E is replaced by E_{eff} and t is replaced by t_{eff}. In particular, using the dimensionless expression for the energy barrier introduced in (2.8) and (6.1) and plotted in Figs. 10 and 12, one finds the following comparison between the energy barrier for sandwich and monocoque shells of the same mass at the same levels of p/p_C (or of $\bar{\sigma}/\sigma_C$)

$$\frac{W_{sandwich}}{W_{monocoque}} = \left(1+3\left(\frac{c}{t}\right)+3\left(\frac{c}{t}\right)^2\right)^{3/2} \tag{7.1}$$

The effect of the bending stiffening enhancement achieved via sandwich construction on increasing the energy barrier is potentially very large. In addition, there is an accompanying increase in the buckling pressure p_C or load of the perfect shell, and the relevant normalization of the imperfection amplitude in the imperfection-sensitivity plots becomes δ/t_{eff} in place of δ/t. Of course, a sandwich shell of the same mass as a monocoque shell will be more susceptible to plastic yielding at the same level of p/p_C and, in addition, sandwich construction is likely to bring into play local buckling modes not present in a monocoque shell. These additional factors must be taken into account in any design involving stiffening. Nevertheless, the dramatic increase of the energy barrier implied by (7.1) sheds further light on the role of stiffening.

References

Berke, L., Carlson, R.L., 1968. Experimental studies of the post buckling behaviour of complete spherical shells. Exp. Mech. 8, 548–553.

Budiansky, B., Hutchinson, J.W., 1979. Buckling: progress and challenge. In: Besseling, J.F., van der Heijden, A.M.A. (Eds.), Trends in Solid Mechanics 1979. Delft University Press, pp. 93–116.

Evkin, A.Y., Krasovskiy, V.L., Manevich, L.I., 1978. Stability of longitudinally compressed cylindrical shells under quasi-static local disturbances. Izv. AN SSSR, Mekh. Tverdogo Tela 13 (6), 95–100.

Evkin, A.Y., Lykhachova, O.V., 2017. Energy barrier as a criterion for stability estimation of spherical shell under uniform external pressure. Int. J. Solids Struct. 118-119, 14–23.

Evkin, A.Y., Kolesnikov, M., Prikazchikov, D.A., 2016. Buckling of a spherical shell under external pressure and inward concentrated load: asymptotic solution. Math. Mech. Solids 1, 1–13.

Friedrichs, K.O., 1941. On the minimum buckling load of spherical shells. In: Theodore Von Kármán, Anniversary Volume: Contributions to Applied Mechanics and Related Subjects By the Friends of Theodore Von Kármán on His Sixtieth Birthday. California Institute of Technology, Pasadena, CA, pp. 258–272.

Haynie, W., Hilburger, M., Bogge, M., Maspoli, M., Kriegesmann, B., 2012. Validation of lower-bound estimates for compression-loaded cylindrical shells. In: Proceedings of 53rd AIAA/ASME/ASCE/AHS/ASC Structures, Structural Dynamics and Materials Conference, Structures, Structural Dynamics, and Materials and Co-located Conferences doi:10.2514/6.2012-1689.

Horak, J., Lord, G.J., Peletier, M.A., 2006. Cylinder buckling: the mountain pass as an organizing centre. SIAM J. Appl. Math. 66, 1793–1824.

Hunt, G.W., Peletier, M.A., Champneys, A.R., Woods, P.D., Ahmer Wadee, M., Budd, C.J., Lord, G.J., 2000. Cellular buckling in long structures. Nonlinear Dyn 21, 3–29. doi:10.1023/A:1008398006403.

Hunt, G.W., Lord, G.J., Peletier, M.A., 2003. Cylindrical shell buckling: a characterization of localization and periodicity. Discr. Contin. Dyn. Syst. B 3, 505–518.

Hutchinson, J.W., 1967. Imperfection sensitivity of externally pressurized spherical shells. J. Appl. Mech. 48–55.

Hutchinson, J.W., 2010. Knockdown factors for cylindrical and spherical shells subject to reduced biaxial membrane stress. Int. J. Solids Struct. 47, 1443–1448.

Hutchinson, J.W., 2016. Buckling of Spherical Shells Revisited. Proc. R. Soc. A 472 (2195), 20160577.

Hutchinson, J.W., Thompson, J.M.T., 2017a. Nonlinear buckling behaviour of spherical shells: barriers and symmetry-breaking dimples. Phil. Trans. R. Soc. A 375, 20160154. doi:10.1098/rsta.2016.0154.

Hutchinson, J.W., Thompson, J.M.T., 2017b. Nonlinear buckling interaction for spherical shells subject to pressure and probing forces. J. Appl. Mech. 84 (June), 061001. doi:10.1115/1.4036355.

Koiter, W.T., 1963. The effect of axisymmetric imperfections on the buckling of cylindrical shells under axial compression. Kon. Neder. Acad. Wet. B 66, 265–279.

Krasovsky, V., Marchenko, V., Schmidt, R., 2011. Deformation and buckling of axially compressed cylindrical shells with local loads in numerical simulation and experiments. Thin-Walled Struct. 49, 576–580.

Kreilos, T., Schneider, T.M., 2017. Fully localized post-buckling states of cylindrical shells under axial compression. Proc. R. Soc. A 473, 20170177. doi:10.1098/rspa.2017.0177.

Lee, A., Marthelot, J., López Jiménez, F., Hutchinson, J.W., Reis, P.M., 2016a. The geometric role of precisely engineered imperfections on the critical buckling load of spherical shells. J. Appl. Mech. 83, 111005 (11 pages).

Lee, A., Brun, P.-T., Marthelot, J., Balestra, G., Gallaire, F., Reis, P.M., 2016b. Fabrication of slender elastic shells by the coating of curved surfaces. Nat. Commun. 7 p. 11155.111005-1-11.

Lord, G.J., Champneys, A.R., Hunt, G.W., 1997. Computation of localized post buckling in long axially-compressed cylindrical shells. In: Champneys, A.R., Hunt, G.W., Thompson, J.M.T. (Eds.), Localization and Solitary Waves in Solid Mechanics, pp. 2137–2150. Special Issue of Phil. Trans. R. Soc., A, 355.

Marthelot, J., López Jiménez, F., Lee, A., Hutchinson, J.W., Reis, P.M., 2017. Buckling of pressurized hemispherical shells subject to probing forces. J. Appl. Mech. 84, 121005.

Mossakovskiy, V.I., Manevich, L.I., Evkin, A.Y., 1975. Investigation of post-buckling equilibrium forms of a compressed cylindrical shell. Prikl. Mekh. 11, 1155–1159.

Seide, P., Weingarten, V.I., Morgan, E.J., 1960. The development of design criteria for elastic stability of thin shell structures. Space Technology Laboratories, Inc., Los Angles, CA Final Report: STL/TR-60-0000-19425 December 1960.

Simitses, G.J., Hodges, D.H., 2006. Fundamentals of Structural Stability. Butterworth-Heinemann.

Starlinger, A., Rammerstorfer, F.G., Auli, W., 1988. Beulen und Nachbeulverhalten von Duennen Verrippten und Unverrippten Kugelschalen Unter Aussendruck. Z. Angew. Math. Mech. 68 (4), 257–260.

Thompson, J.M.T., 2015. Advances in shell buckling: theory and experiments. Int. J. Bifurc. Chaos 25 (1), 1530001. (25 pages). doi: 10.1142/S0218127415300013.

Thompson, J.M.T., van der Heijden, G.H.M., 2014. Quantified "shock-sensitivity" above the Maxwell load. Int. J. Bifurc. Chaos 24 (3), 1430009. doi:10.1142/S0218127414300092.

Thompson, J.M.T., Sieber, J., 2016. Shock-sensitivity in shell-like structures: with simulations of spherical shell buckling, Int. J. Bifurcation and Chaos 26 (2), 1630003. (25 pages). doi: 10.1142/S0218127416300032.

Tsien, H.S., 1942. Theory for the buckling of thin shells. J. Aeronaut. Sci. 9, 373–384.

Virot, E., Schneider, T., Rubinstein, S.M., 2017. Stability landscape in shell buckling. Phys. Rev. Lett. 119, 224101. doi:10.1103/PhysRevLett.119.224101.

Wagner, H.N.R., Huhne, C., Niemann, S., Khakimova, R., 2017. Robust design criterion for axially loaded cylindrical shells-simulation and validation. Thin-Walled Struct. 115, 154–162.

Wang, B., Hao, P., Li, G., Fang, Y., 2013. Determination of realistic worst imperfections for cylindrical shells using surrogate model. Struct. Multidisc. Optim. 48, 777–794.